Ionospheric convection in the postnoon auroral oval: Super Dual Auroral Radar Network (SuperDARN) and polar ultraviolet imager (UVI) observations

A. Kozlovsky,[1,2] A. Koustov,[3] W. Lyatsky,[4] J. Kangas,[1] G. Parks,[5] and D. Chua[6,7]

[1] Super Dual Auroral Radar Network (SuperDARN) observations, ultraviolet imaging from the Polar satellite (ultraviolet imager [UVI]), and particle precipitation data from Defense Meteorological Satellite Program (DMSP) satellites have been used to investigate the electrodynamics of the postnoon auroral oval in the Northern hemisphere. We show that: (1) For negative interplanetary magnetic field (IMF) By, the convection reversal (CR) was colocated with the maximum of auroral luminosity, but during positive IMF By, the convection reversal was poleward of the auroral oval up to several degrees in latitude. (2) Postnoon auroral oval was associated with a large-scale upward field-aligned current (FAC) of the order of 6×10^{-7} A m^{-2} in magnitude (the FAC was inferred from the SuperDARN and UVI data). For negative IMF By, the maximum of the auroral intensity coincides in latitude with the maximum of the upward FAC. However, for positive IMF By, the maximum of the upward FAC was shifted to the poleward edge of the auroral oval. (3) In response to the IMF By turning from positive to negative, the maximum of the auroral luminosity did not change its position noticeably, but the position of the CR changed considerably from $80°-81°$ to about $76°$ magnetic latitude (MLAT), and the maximum of FAC moved from $77°-78°$ to about $76°$ MLAT. Thus, after the IMF By turns negative, both the FAC maximum and CR tend to coincide with the auroral maximum. (4) The IMF Bz positive deflection was followed by a decrease in both FAC intensity and auroral luminosity. However, the decrease in the auroral luminosity lags behind the FAC decrease by about 12 min. Firstly, these observations allow us to suggest that the IMF By-related electric field can penetrate into the closed magnetosphere and produce convection and FAC changes in the region of the postnoon auroral oval. Secondly, we suggest that the interchange instability is a promising mechanism for the postnoon auroras. *INDEX TERMS:* 2463 Ionosphere: Plasma convection; 2407 Ionosphere: Auroral ionosphere (2704); 2708 Magnetospheric Physics: Current systems (2409); 2784 Magnetospheric Physics: Solar wind/magnetosphere interactions; *KEYWORDS:* postnoon aurora, ionospheric convection, field-aligned currents, IMF changes, boundary plasma sheet

[1] Sodankylä Geophysical Observatory, Sodankylä, Finland.
[2] Department of Physical Sciences, University of Oulu, Oulu, Finland.
[3] Department of Physics and Engineering Physics, University of Saskatchewan, Saskatoon, Saskatchewan, Canada.
[4] Department of Physics, Alabama A&M University, Normal, Alabama, USA.
[5] Space Science Laboratory, University of California, Berkeley, California, USA.
[6] Department of Earth and Space Sciences, University of Washington, Seattle, Washington, USA.
[7] Now at Naval Research Laboratory, Washington, District of Columbia, USA.

1. Introduction

[2] The maximum of the dayside auroral luminosity occurs in the postnoon region, around 14–16 MLT [*Snyder and Akasofu*, 1976; *Shepherd et al.*, 1976; *Cogger et al.*, 1977; *Liou et al.*, 1997]. Multiple bright discrete arcs related to the so-called "14 MLT" region have been first identified by *Murphree et al.* [1981] and later by *Evans* [1985]. *Meng and Lundin* [1986] examined the morphology of the dayside auroral oval by using auroral images from the Defense Meteorological Satellite Program (DMSP) satellites. The auroral displays were grouped into five characteristic types, depending on the geomagnetic activity and the Bz component of the interplanetary magnetic field (IMF).

[3] Recent data indicate that the postnoon auroral arcs are most likely associated with the dayside extension of the plasma sheet and the boundary between the plasma sheet and other regions [*Lu et al.*, 1995; *Troshichev et al.*, 1996; *Liou et al.*, 1999]. Another possible source region for the postnoon aurora is the low-latitude boundary layer (LLBL), including the outer part of the plasma sheet [*Murphree et al.*, 1981; *Ohtani et al.*, 1995].

[4] The postnoon arcs are located in the region of convection shear within the large-scale Region 1 field-aligned currents where focusing of the convection cell occurs [e.g., *Lui et al.*, 1989; *Bythrow et al.*, 1994; *Ohtani et al.*, 1995]. Ultraviolet imaging from Polar shows that the dayside auroral emission is enhanced by sunlight [*Liou et al.*, 1997]. This result demonstrates an important role played by the ionospheric conductivity and connection of the aurora with the magnetosphere–ionosphere current system. Below we list briefly some key unresolved problems related to the electrodynamics of the postnoon auroral oval.

1.1. Field-Aligned Currents and Postnoon Auroras

[5] The maximum of the Region 1 upward field-aligned current (FAC) takes place in the afternoon sector [*Iijima and Potemra*, 1976a, 1976b; *Bythrow et al*, 1994]. To maintain the field-aligned currents, acceleration processes may be excited, which result in auroral luminosity. The spatial structure of the dayside large-scale field-aligned current systems was examined by using Viking and DMSP-F7 data [*Ohtani et al.*, 1995]. The Region 1 system was found to be located in the core part of the auroral oval and confined to a relatively narrow range of latitudes that includes the convection reversal.

[6] Physical mechanisms of the large-scale field-aligned currents have been reviewed by, e.g., *Troshichev* [1982] and *Potemra* [1994]. For the magnetospheric sources of the field-aligned currents, three basic current systems associated with different generation mechanisms have been suggested:

1. The solar wind dynamo mechanism in the open polar cap [*Dungey*, 1961], in which case the field-aligned currents are closed by the transverse inertial currents in the magnetic field lines connected to the solar wind. The southward (negative) IMF Bz produces two convection vortices with foci at the polar cap boundary. Corresponding downward and upward field-aligned currents flow in the dusk and dawn parts of the polar cap, respectively. IMF By generates an electric potential difference between the two polar caps, which comes from the solar wind, so that field-aligned currents flow between the hemispheres (more details can be found in the work of *Burch et al.* [1985]). In the northern polar cap, the plasma flows are westward (eastward) for positive (negative) IMF By.

2. The viscous interaction of the solar wind with the magnetosphere [*Axford and Hines*, 1961] operates in the vicinity of the magnetopause and drives field-aligned currents on closed magnetic field lines. The enclosing transverse drift electric currents are due to the viscosity.

3. Gradient drift currents in hot magnetospheric plasma, which drive field-aligned currents when crossing plasma boundaries in the inner magnetosphere [*Vasyliunas*, 1970]. The gradient drift currents produce polarization effects and field-aligned currents in the magnetospheric regions where gradients of plasma pressure exist (more detail discussion is given below in section 7). As it has been shown [*Troshichev*, 1982; *Yamamoto et al.*, 1996; *Iijima et al.*, 1997; *Shiokawa et al.*, 1998], the plasma pressure gradients can be an effective source of field-aligned currents in the low-latitude boundary layer as well as in the plasma sheet.

[7] Generally, all three mechanisms may contribute to the Region 1 field-aligned current [*Potemra*, 1994]. However, the relationship between the FACs and auroral precipitations is not yet well established.

1.2. Does the Postnoon Aurora Coincide With the Convection Reversal?

[8] The postnoon auroral activity often consists of separate bright spots that may be explained by the Kelvin–Helmholtz instability in the convection shear region [*Lui et al.*, 1989]. From the DMSP satellite data, *Troshichev et al.* [1996] observed the convection shear within the auroral oval. This agrees with the earlier result of *Bythrow et al.* [1981] who used the Atmosphere Explorer C low-altitude satellite data and found the convection reversal boundary inside the Region 1 field-aligned current.

[9] The Svalbard EISCAT radar and Polar satellite ultraviolet imager data have been used to investigate structure and dynamics of the postnoon auroral oval [*Kozlovsky and Kangas*, 2001]. The EISCAT data on ion velocity and temperature together with ground magnetometers showed that the auroras were located in the region of convection shear. On the other hand, *Moen et al.* [1994] monitored auroral structures by ground-based instruments and found that the postnoon auroras locate predominantly on the sunward convecting field lines equatorward of the convection reversal boundary.

1.3. IMF Control of the Postnoon Aurora, Convection, and FAC

[10] *Liou et al.* [1998] studied the 13–18 MLT region statistically using Polar (UV imager) and WIND (solar wind and IMF) satellite data. They concluded that the solar wind dynamic pressure, density, and speed do not significantly affect the total intensity of the afternoon aurora, whereas enhancement of the afternoon aurora occurs for a large transverse component of the IMF and for the away (from the Sun) component of the IMF Bx. *Kozlovsky and Kangas* [2001] studied the response of the aurora to southward turnings of the interplanetary magnetic field. Response of the high-latitude convection to IMF variations is a topic of numerous papers using Super Dual Auroral Radar Network (SuperDARN) radars [see, e.g., *Ruohoniemi and Greenwald*, 1996, 1998; *Taylor et al.*, 1998; *Kustov et al.*, 1998, and references therein]. However, the above observations do not allow the investigation of the responses of the auroral oval to the convection and FAC changes initiated by IMF variations.

1.4. Aims of the Study

[11] We use the ultraviolet imager (UVI) onboard Polar satellite and Super Dual Auroral Radar Network (Super-DARN) radars to observe the auroral oval together with the ionospheric convection in a large area from 65° to 90° in latitude and from 13 MLT to 18 MLT in longitude with ∼10-min resolution. We focus on the location of the

Table 1. Solar Wind Propagation Time

Day	UT	GSM Wind Position, R_E			Solar Wind Velocity, km s^{-1}	Propagation Time to the Ionosphere, min
		X	Y	Z		
17 January	2030–2200	135.5	−34.5	−25.2	320	47
3 February	2140–2220	188.4	2.2	−18.6	370	57
22 February	1950–2030	212.2	20.0	−3.8	390	61
14 March	2130–2210	226.5	15.9	13.5	380	67

postnoon aurora with respect to the convection reversal, on the distribution of field-aligned currents in the afternoon, and the relative positioning of the aurora and convection during IMF variations.

[12] The paper is organized as follows. The instruments used and methods of the data analysis are described in section 2. Section 3 gives the general description of the cases under investigations. Convection reversal boundary locations and field-aligned current distributions are studied in sections 4 and 5, respectively. Section 6 is devoted to the investigation of the aurora, convection, and FACs response to IMF variations. In section 7, interpretation and discussion of the results are presented.

2. Instruments and Methods

2.1. Polar UVI

[13] The ultraviolet imager onboard the Polar satellite allows observations of the whole auroral oval with about 1 min temporal and 40-km spatial resolutions [*Torr et al.*, 1995]. In some cases, wobbling of the satellite can considerably degrade the spatial resolution, whose effects are discussed below in section 3. To support the auroral oval location obtained from the UVI, we use the electron precipitation data from the DMSP low-altitude satellites (section 2.4).

[14] We use images obtained in the N_2 Lyman–Birge–Hopfield (LBH) emission in a wavelength band near 170 nm (LBHL bands). The images were selected from the Coordinated Data Analysis Web (http://cdaweb.gsfc.nasa.gov/), which provides one frame in 6–8 minutes. In the selected images, dayglow has been removed and line of sight corrections have been done (see, e.g., *Newell et al.* [2001] for more details). The assumed altitude of the LBH emissions is 120 km. The count rate (photons cm^{-2} s^{-1}) observed by the Polar UVI can be converted to a surface brightness in Rayleighs by multiplying by factor 30.2 [e.g., *Newell et al.*, 2001]. Using data on the Polar satellite position, attitude, and UVI pointing, we map the UVI data into geographic coordinates. Then the geographic coordinates of the pixels are transformed into Altitude Adjusted Corrected Geomagnetic coordinates (AACGM) that are commonly used in SuperDARN related studies. The AACGM coordinate system is a synthesis of the Corrected Geomagnetic Coordinate System [*Gustafsson et al.*, 1992] and the PACE [*Baker and Wing*, 1989] geomagnetic coordinate system. Any two points connected by a magnetic field line have the same magnetic latitude (MLAT) and longitude in the AACGM coordinate system.

2.2. SuperDARN

[15] SuperDARN is a network of high-frequency (HF) coherent radars monitoring plasma convection in a significant portion of the high latitude ionosphere. In the northern hemisphere, the radars cover magnetic latitudes of $65°–85°$ and more than half of the globe in longitude. A detailed description of the system was given by *Greenwald et al.* [1995]. The SuperDARN radars are sensitive to F region electron density irregularities with scale sizes of $10–15$ m. At the F region heights, such irregularities move with the convection velocity ($\mathbf{E} \times \mathbf{B}$ drift) so that the Doppler shift of received signal is the line-of-sight component of the convection velocity. By combining measurements from all radars a global scale convection map can be obtained with a time resolution of 2 min.

[16] In the present study, we consider data from six radars located in Canada (Saskatoon, Kapuskasing, and Goose Bay), Iceland (Stokkseyri and Pykkvybaer), and Finland (Hankasalmi). The radars are positioned along $\sim60°$ geomagnetic latitude in the longitudinal range from $47°$ W to $103°$ E (AACGM). Imaging the large-scale convection is done using the fitting technique described by *Ruohoniemi and Baker* [1998]. The spatial resolution of these measurements is of the order of 100 km. We consider convection patterns averaged over 10 min. Thus, the spatial and temporal resolutions of SuperDARN convection measurements and Polar UVI luminosity observations are comparable.

2.3. IMF and Solar Wind Data

[17] The Wind satellite provided interplanetary magnetic field (IMF) and solar wind (SW) velocity and plasma density data upstream in front of the magnetosphere. Locations of the satellite are shown in Table 1 together with the solar wind transit times to the ionosphere. The transit time of the solar wind from the satellite to the Earth's bow shock subsolar point was estimated by $\Delta t_{sw} = (X_{sc} - X_{bs})/V_{sw}$, where X_{sc} is the coordinate of the Wind satellite, $X_{bs} = 14.6$ R_E is the coordinate of the subsolar bow shock [*Fairfield*, 1971], and V_{sw} is the solar wind velocity. The total delay time to the ionosphere is the sum of this transit time plus 5 min needed for disturbance to pass the magnetosheath and 2 min Alfvén transit time required to reach the ionosphere [*Lockwood et al.*, 1989]. The Wind satellite was at a distance of $20–40$ R_E from the Earth–Sun line, so the uncertainty in the delay time is approximately 10 min as *Ridley* [2000] has shown.

2.4. Particle Precipitation Data From DMSP Satellites

[18] DMSP satellites are in a low altitude (830 km) polar orbit and the orbital period is 101 min. The Precipitating Electron and Ion Spectrometers SSJ/4 onboard the satellites provide a complete energy spectrum of electron and ion particle fluxes between 30 eV and 30 keV recorded every second. We use data from the DMSP F13 satellite, which crossed the postnoon auroral oval to identify dayside boundaries [*Newell et al.*, 1991] and to
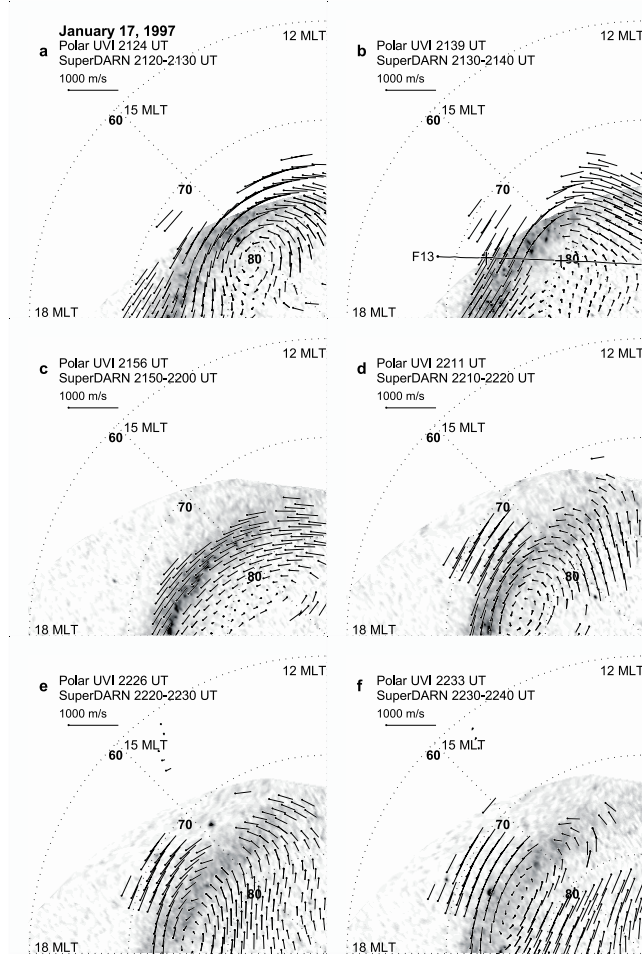
Figure 1. A sequence of diagrams for event on 17 January shows change in convection.

support and substantiate the oval locations derived from Polar UVI.

3. Observations

[19] We have examined the Polar UVI and SuperDARN data obtained in January, February, and March of 1997. From these data we selected cases for which the postnoon auroral oval was seen well in the UV images and the SuperDARN convection measurements were available in significant portions of the postnoon aurora. Four proper events have been identified for the study. In all cases, the Polar satellite was at a distance of about 8 R_E over the northern polar cap.

[20] Because of the wobbling, UVI images sometimes are streamed in approximately noon–midnight direction, which leads to an uncertainty up to 400 km along the streaming, in the worst case. When this effect takes place, bright auroral structures in the images are clearly stretched along the wobble line (see, e.g., the case of 1255 UT on 12 March 1997, presented by *Kozlovsky and Kangas* [2001]). In the images investigated in the present study, there is no visible evidence of the streaming caused by the wobbling effect. However, even if the streaming did occur, it would not have significantly affected the location of the postnoon auroral

oval because the wobbling was along the 10–22 MLT line, which is along the auroral oval around 16 MLT. (This direction of streaming can be seen in many images obtained during January–March 1997, which period we study.) For the same reasons, the wobbling should not affect the auroral intensity averaged over local time in the 14–17 MLT range, whose characteristic we analyze. Additionally, to support the auroral oval location, we used the electron precipitation data from the DMSP low-altitude satellites.

3.1. Case of 17 January 1998

[21] On 17 January, a sequence of eight convection plots was obtained at 2120–2240 UT, and nine UVI frames were used to monitor the auroral oval. The event is represented by a sequence of six diagrams in Figure 1 where the auroral images are overlaid with convection vectors. DMSP F13 satellite crossed the postnoon auroral oval at about 2137–2140 UT. The trajectory of the satellite is shown in the frame taken at 2139 UT (Figure 1b), and the spectrogram of the electron precipitation along the trajectory is presented in Figure 2. The solid line on the spectrogram shows the ultraviolet intensity along the trajectory. There is a good correspondence between the UV brightness and the energy flux of the electron precipitation, which supports the accuracy of UVI mapping. Vertical dashed lines in Figure 2 indicate sharp edges of the postnoon precipitation region, which is also indicated in Figure 1b by crosses at the satellite trajectory. The postnoon auroral oval was associated with the boundary plasma sheet (BPS) and low-latitude boundary layer (LLBL) that was deduced from the electron and ion (not shown here) precipitation data accordingly to the definition of *Newell et al.* [1991]. These plasma boundaries are indicated on the top of Figure 2.

[22] Interplanetary parameters are shown in Figure 3 where vertical dash lines with letters that indicate the times of the UVI frames denoted by corresponding letters in Figure 1 (the solar wind propagation time was taken into account). The IMF was relatively stable one hour prior to the event, and Bz and By components were about −2 nT and +2 nT, respectively. At 2120 UT, IMF By changed suddenly from positive to negative and also a short positive deflection in Bz IMF was evident. This disturbance reached the ionosphere at about 2200–2210 UT. The solar wind pressure was stable around 4 nPa.
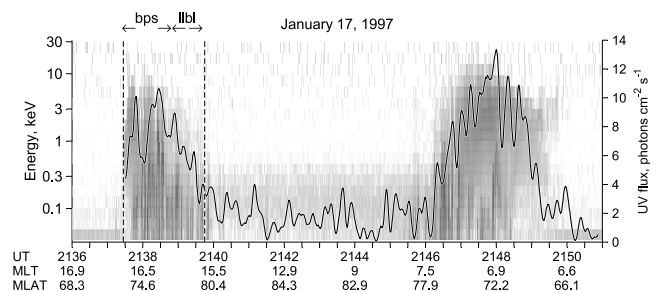

Figure 2. Spectrogram of the electron precipitation measured by the DMSP satellite. Solid line on the spectrogram shows the ultraviolet intensity along the satellite trajectory. Vertical dashed lines indicate sharp edges of the postnoon precipitation region, which are also indicated in Figure 1b by crosses at the satellite trajectory.
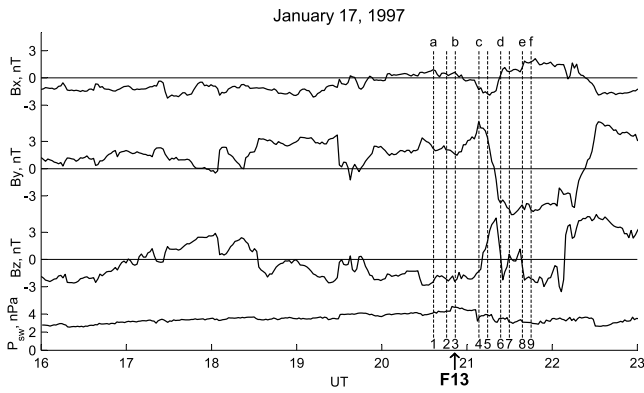
Figure 3. Interplanetary magnetic field and solar wind dynamic pressure for the event of 17 January. Vertical dashed lines with letters indicate moments of the UVI frames in Figure 1. The arrow indicates time of the DMSP F13 satellite flight. The solar wind propagation time was accounted.

[23] The width of the postnoon auroral oval was of the order of 200–300 km and maximum of the luminosity was located around 76° MLAT in the 14–17 MLT sector. The position of the auroral oval did not change noticeably in the course of the IMF change. At 2124 UT the convection reversal boundary was located approximately 500 km poleward of the maximum in auroral luminosity (Figure 1a). Until 2210 UT the whole postnoon auroral oval was in the region of the westward (sunward) flow (Figures 4a–4d). The IMF By change was accompanied by a motion of the convection reversal from 81° to 76° between 2210 UT and 2220 UT. At 2233 UT the maximum of luminosity was coinciding with the convection reversal (Figure 4f). After 2240 UT, observations of the convection were not available at the auroral oval location and poleward of it.

3.2. Three Cases of IMF By < 0

[24] In three events, 3 February, 22 February, and 14 March, data coverage was good for both UVI and Super-DARN during about 30 min that allowed observations of several (2 or 3) consecutive diagrams. However, in these cases both the auroral oval and convection did not change much during the observations so these events are represented by single a diagram in Figure 4.

[25] The interplanetary parameters are shown in Figure 5. On 3 February, the observations were obtained soon after a sharp IMF Bz jump from about zero to −3 nT. By was negative, about −1 nT. On 22 February, the IMF was stable during one hour before the observations, Bz and By were negative around −3 nT and −5 nT, respectively. On 14 March, the IMF was variable during the observations, with Bz between −1 nT and −5 nT, and By around −5 nT. Thus all these events were during negative IMF By and Bz. The solar wind pressure was stable around 1–2 nPa in all these cases.

[26] On 3 February, the auroral oval in 15–18 MLT appeared as a narrow (100–200 km width) bright arc at 78° MLAT, which corresponds to Type 4 auroral oval ("extended bright afternoon and evening arc") in the classification of *Meng and Lundin* [1986]. In other two cases, the auroral oval in 14–16 MLT was seen in the Polar UVI as a 100–200 km width strip of enhanced luminosity

stretched at about 75° MLAT. In all these three cases, the convection reversal occurred at the auroral oval center to within a 100-km accuracy.

[27] DMSP F13 satellite crossed the postnoon auroral oval 24 min after the UVI frame, 18 min before the UVI frame, and 47 min before the UVI frame for the cases of 3 February, 22 February, and 14 March, respectively (arrows in Figure 5 indicate times of the satellite flights). The trajectories of the satellite and spectrograms of the electron precipitation along the trajectory are shown in Figure 4, where dashed lines on the spectrograms and crosses at the satellite trajectory indicate sharp edges of the postnoon precipitation region. The solid line on the spectrogram shows the ultraviolet intensity along the trajectory. Taking into account the time differences and the IMF variations, the correspondence between the UV brightness and electron precipitations is good enough to support the accuracy of the
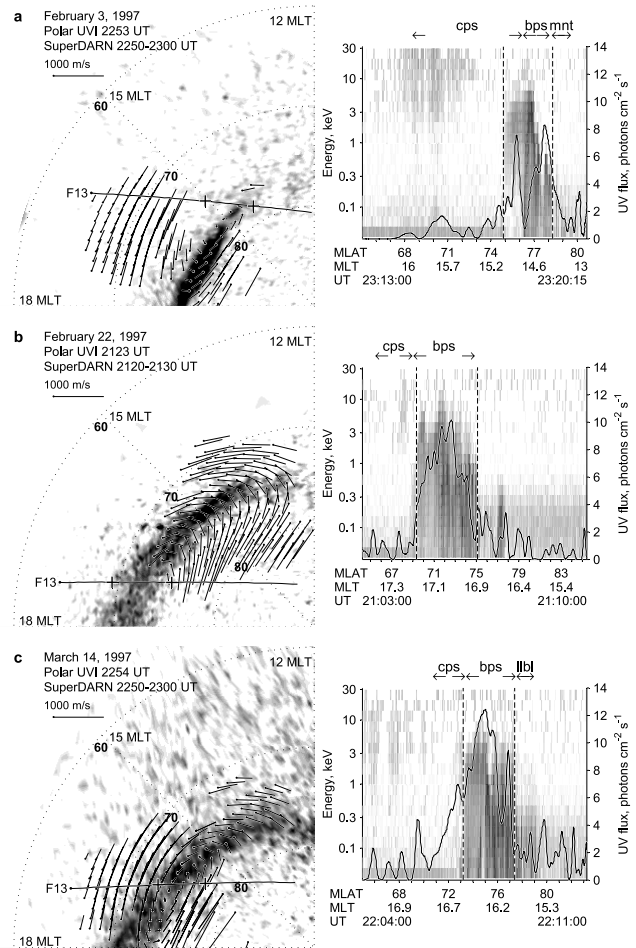

Figure 4. Three cases of the postnoon auroral oval observations by Polar UVI and ionospheric convection measurements by SuperDARN. Trajectory of DMSP F13 satellite is shown in the frames, and the spectrogram of the electron precipitation measured by the DMSP satellite are presented in the right. Solid lines on the spectrograms show the ultraviolet intensity along the satellite trajectory. Vertical dashed lines indicate sharp edges of the postnoon precipitation region, which are also indicated in the UV frames by crosses at the satellite trajectory.
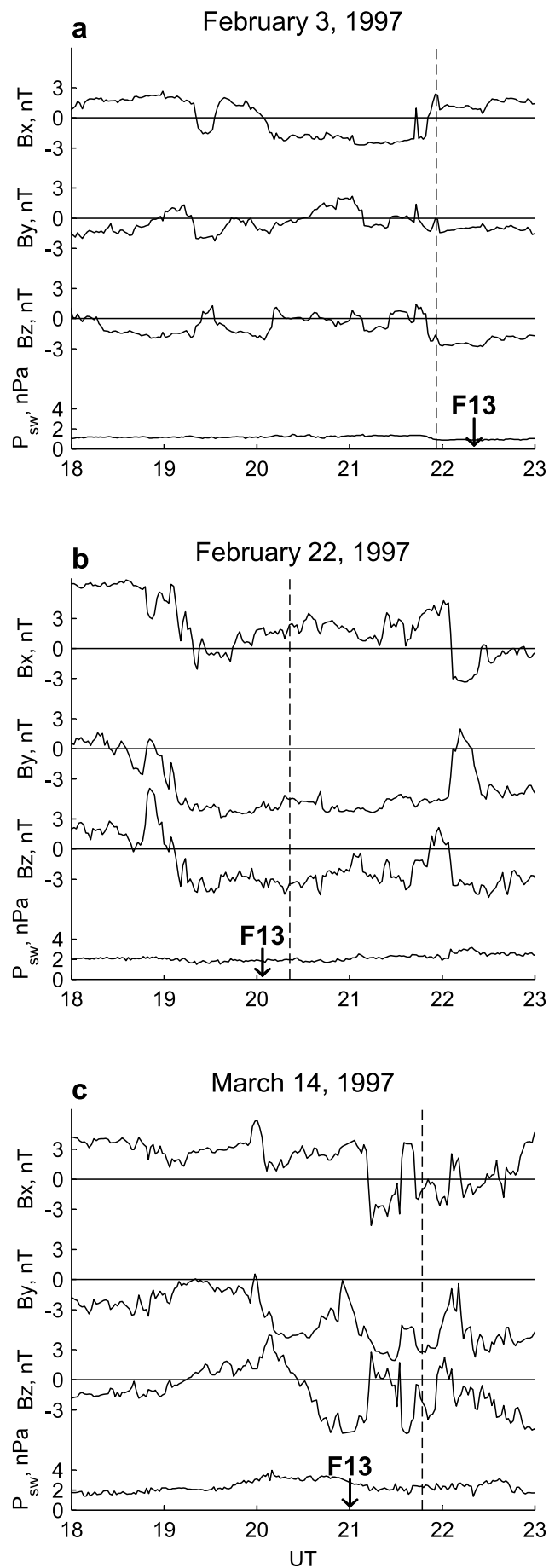
UVI mapping. The postnoon auroral oval was mostly associated with BPS (the plasma boundaries inferred from DMSP data are indicated on the spectrograms in Figure 4).

4. Postnoon Aurora and Convection Reversal

[28] Table 2 summarizes the characteristics of the events described in section 3. All of the events were associated with negative IMF Bz from −2 nT to −4 nT. The postnoon auroral oval was observed as a strip of 200- to 400-km width. The postnoon auroral oval was mostly associated with particle precipitation from the BPS. In all cases, except for one event (17 January, 2120–2210 UT), the convection reversal was observed at the center of the postnoon auroral oval to within 1° of latitude. For the exceptional case, the convection reversal was well poleward of the auroral oval. For this event, IMF By was positive whereas it was negative for all other events. For this special event, somewhat later, after IMF By turned to negative values, the convection reversal moved to the center of the auroral oval.

[29] In further analysis, we consider meridional cross-sections of the afternoon auroral luminosity and convection (centered around 15.5 MLT). To obtain them, we averaged over local time the auroral intensity and plasma flow (east-ward and northward components) in the range of 14–17 MLT. As was discussed above in section 3, this is averaging over about 1200 km along the direction of possible wob-bling of the Polar satellite. The MLT-averaged auroral luminosity was not affected by the wobbling.

[30] Figure 6 shows the averaged parameters versus latitude for the events described above. Dots show auroral intensities from the UVI pixels versus latitude, and the solid lines present the averaged distributions obtained from the pixel values. Vectors on the top of the plots indicate the plasma velocity, and vertical dashed lines indicate locations of the convection reversal. Figure 6 shows that for positive By (2124 UT on 17 January) the CR was 5° poleward of the maximum of auroral luminosity whereas for negative By (cases of 17 January (2233 UT), 3 February, 22 February, and 14 March) the maximum of auroral intensity coincided with CR. The response of CR to the IMF By change will be considered later in section 6.

5. Field-Aligned Currents

[31] In this section we study the field-aligned currents in the vicinity of the postnoon auroral oval. The field-aligned current, $j_\parallel$, can be estimated from the divergence of the height-integrated transverse (perpendicular to the magnetic field) ionospheric currents,

$$j_\parallel = \nabla_\perp \cdot \mathbf{J}_\perp, \qquad (1)$$

where

$$\mathbf{J}_\perp = \Sigma_P \mathbf{E}_\perp + \Sigma_H [\mathbf{e}_z \times \mathbf{E}_\perp]. \qquad (2)$$

Figure 5. (opposite) Interplanetary magnetic field and solar wind dynamic pressure for the events presented in Figure 4. Vertical dashed lines indicate the moments of optical-radar comparisons. Arrows indicate times of the DMSP F13 satellite flights. The solar wind propagation time was accounted.

Table 2. Characteristics of the Postnoon Auroral Oval and IMF Conditions

Day	UT	Maximum Level of Auroral Intensity MLT	Maximum Level of Auroral Intensity MLAT, °	Distance to CR, ° of Latitude	Magnetospheric Region	IMF, nT Bx	IMF, nT By	IMF, nT Bz
17 January	2124	14−18	74−77	5	BPS, LLBL	+1	+2	−2
17 January	2233	14−16	75−76	<1		+2	−5	−2
3 February	2253	15−18	78	<1	CPS, BPS	+2	−1	−2
22 February	2123	14−16	74	<1	BPS	+2	−5	−3
14 March	2254	14−16	74−75	<1	BPS	var.	−5	−3

Here Σ_P and Σ_H are the Pedersen and Hall height-integrated ionospheric conductivities, $\mathbf{E}_\perp$ is the transverse component of the electric field $\mathbf{E}$, and $\mathbf{e}_z$ is a unit vector along the magnetic field. In the ionosphere, the electric field component along $\mathbf{e}_z$ is assumed to be zero, and the electric field is vortex-free,

$$\text{curl}(\mathbf{E}) = 0. \quad (3)$$

[32] Figures 1 and 4 illustrate that spatial variations of the auroral luminosity and convection velocity are much larger across the oval than along it. For this reason we neglect all spatial changes along the east–west direction and consider only the one-dimensional characteristics (across the oval). In this case, equations (1), (2), and (3) give

$$j_\parallel = \frac{\partial}{\partial x}(\Sigma_P E_x) - E_y \frac{\partial}{\partial x}\Sigma_H, \quad (4)$$

where x and y axis are directed to the north and east, respectively. The electric field components can be derived from the plasma velocity maps measured by the Super-DARN radars.

[33] The ionospheric conductivity may be represented as a sum of two components. The first one, denoted below as Σ_{P0} and Σ_{H0}, is a background conductivity, which is mainly due to photoionization. For our estimations, we use an ionospheric conductivity model from the World Data Center for Geomagnetism in Kyoto (http://swdcdb.kugi.kyoto-u.ac.jp/sigcal/index.html). The conductivity model is based on the International Reference Ionosphere (IRI-90) model, which provides ionospheric parameters in the nonauroral ionosphere for magnetically quiet conditions. Dashed lines in Figure 7 show the model Pedersen conductance versus latitude calculated at 15.5 MLT for January, February, and March.

[34] The second component of the ionospheric conductivity, $\Sigma_{P(aur)}$ and $\Sigma_{H(aur)}$, is due to ionization by auroral precipitation and estimated from the flux and energy of precipitating electrons. According to *Robinson et al.* [1987]

$$\Sigma_{P(aur)} = \frac{40\langle E\rangle}{16 + \langle E\rangle^2}F_E^{1/2}, \quad (5)$$

and

$$\frac{\Sigma_{H(aur)}}{\Sigma_{P(aur)}} = 0.45\langle E\rangle^{0.85}, \quad (6)$$

where F_E and $\langle E\rangle$ is the incident energy flux (mW/m^2) and average energy (keV) of the precipitating electrons in the range 500 eV to 30 keV. We shall derive the characteristics

of the precipitation by combining the UVI and DMSP data selected above.

[35] The average energies of the electron precipitating into the postnoon auroral oval have been calculated from the
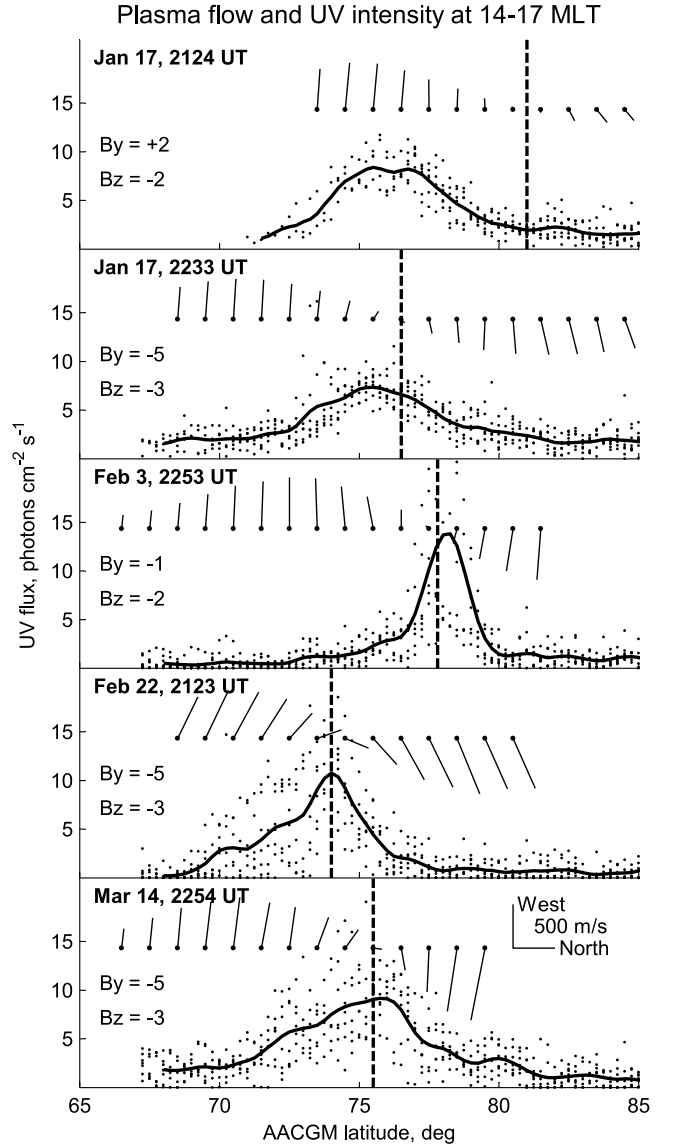

Figure 6. Averaged plasma flow vectors and auroral luminosity versus latitude in 14–17 MLT sector. Vertical dashed lines indicate locations of the convection reversal, dots are auroral intensities from UVI pixels at given latitudes, and solid lines present the averaged distributions obtained from the pixel values.
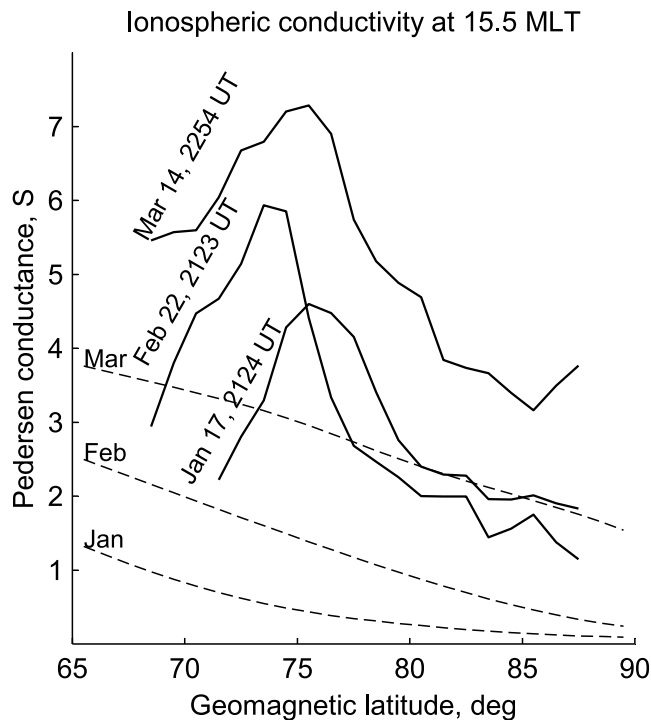
Ionospheric conductivity at 15.5 MLT

Figure 7. The Pedersen conductance versus latitude calculated by equation (9) for some days in January, February, and March (solid lines). Dashed lines show the model Pedersen conductance calculated at 15.5 MLT for the same months.

spectrograms presented in Figures 2 and 4. Additionally, we consider the DMSP data from previous or/and next satellite orbits so that in each case the mean energies were obtained both before and after the investigated events. These observations are summarized in Table 3 where the times (UT) and regions (MLT and AACGM latitude) of the auroral oval crossings are also presented. Table 1 shows that mean energy of the postnoon electron precipitation varied from 1 to 2 keV having a typical value of 1.2 keV, which we shall use in our calculations.

[36] The incident energy flux can be derived from satellite ultraviolet images. In practice, the LBHL emission is essentially independent of the average energy and linearly dependent on the energy flux of precipitating electrons [e.g., *Germany et al.*, 1998]. In the images under consideration, the dayglow removal and line of sight corrections have been done, so one needs only to multiply the UVI brightness by some factor for the F_E calculation. This factor depends on the properties of the atmosphere and can be derived from modeling. *Germany et al.* [1998] has obtained that modeled LBHL column brightness 110 Rayleighs corresponds to the incident energy flux of 1 mW m^{-2}, which depends weakly on the mean energy. Thus, for the mean energy of 1.2 keV we obtain from (5) and (6)

$$\Sigma_{P(aur)} = 5.3(I_{LBHL})^{1/2}, \tag{7}$$

and

$$\Sigma_{H(aur)} = 0.52\, \Sigma_{P(aur)}, \tag{8}$$

where I_{LBHL} is surface brightness in Rayleighs (for the Polar UVI, 1 photons cm^{-2} s^{-1} corresponds to 30.2 R). This relation will be used below in our calculations.

[37] The total ionospheric conductances are sum of two parts,

$$\Sigma_P = \Sigma_{P0} + \Sigma_{P(aur)} \text{ and } \Sigma_H = \Sigma_{H0} + \Sigma_{H(aur)}. \tag{9}$$

[38] We used the average auroral intensity and plasma velocity shown in Figure 6 to calculate field-aligned currents. The solid lines in Figure 7 show the Pedersen conductance versus latitude calculated by (7) and (9) for some days in January, February, and March. The emission rate was of the order of 60–400 R (2–12 photons cm^{-2} s^{-1}) that gives Pedersen conductance of the order of 1.5–3.5 S. This is much larger than the background values 0.5 S at 75° MLAT in January and of the same order as the background conductivity in March. Thus, the second terms in formulae (9) are dominating in the case of 17 January.

[39] The solid lines in Figure 8 (the same as in Figure 6) show the auroral intensities versus latitude that were used for the calculations of ionospheric conductances. Field-aligned currents (calculated by (4)–(10)) versus latitude are presented in Figure 8 as dashed lines and open circles. The plots used reverse axis direction for the field-aligned currents (negative values correspond to an upward current and the electrons coming into the ionosphere). Since the field-aligned currents were obtained from the data averaged over time (10 min), local time sector (14–17 MLT), and latitude (1°), Figure 8 represents large-scale currents in the postnoon sector of the auroral oval. The postnoon auroral oval was associated with the upward field-aligned current, and downward field-aligned current was observed equatorward of the auroral oval.

[40] Figure 8 shows three cases of negative IMF By. One can see that the maximum of the upward FAC (dashed lines

Table 3. Averaged Energy of the Precipitating Electrons (for E > 460 eV)

Polar UVI Date and UT	DMSP				
	UT	MLT	MLAT	E, keV	Regions
17 January/2139	1956:25–1957:59	17.3–17.0	72.8–78.4	1.5	
	2133:41–2135:07	16.6–15.7	72.9–79.8	1.2	BPS, LLBL
	2316:40–2318:15	15.2–13.9	74.0–78.5	1.0	
3 February/2253	2133:41–2135:07	16.7–16.2	73.0–77.4	1.2	
	2316:40–2318:15	15.1–14.1	74.9–78.3	2.1	CPS, BPS
22 February/2123	2104:27–2106:12	17.2–16.8	69.3–75.1	1.2	BPS
	2246:16–2247:33	16.2–15.8	70.1–73.6	1.0	
14 March/2254	2206:40–2208:10	16.5–16.0	73.2–77.4	1.0	BPS
	2349:00–2350:50	15.4–14.5	72.0–76.2	1.2	

UV intensity and field-aligned currents at 14-17 MLT
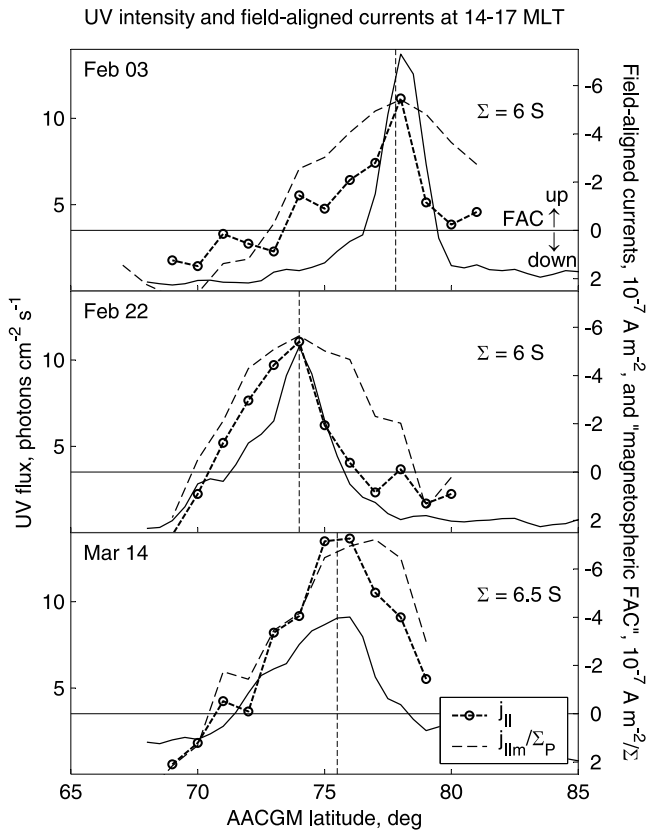

Figure 8. Large-scale field-aligned currents in the post-noon auroral oval (dashed lines with open circles) versus latitude for events presented in Figure 4. The plots use reverse axis direction for the field-aligned currents (negative values correspond to an upward current). Solid lines show the auroral intensities (the same as in Figure 6). Vertical dashed lines indicate positions of the convection reversals. Thin dashed lines show the "magnetospheric component" of FAC $j_{\|m}/\Sigma_P$ corresponding to the Pedersen conductance values indicated in the plots.

with open circles) is of the order of 0.6×10^{-6} A m^{-2} and it is located at the same latitudes as the maximum of auroral intensity (solid lines). Vertical dashed lines indicate here positions of the convection reversals, which coincides well with peaks of both the FAC and auroral luminosity.

[41] Figure 9 uses the same format as in Figure 8 and shows a sequence of plots obtained for the event of 17 January when the IMF By was changing sign from plus (top panels) to minus (bottom panels). The two bottom panels demonstrate the same features as the cases in Figure 8, also obtained for negative IMF By, i.e., the postnoon maximum of auroral intensity coincides with the FAC maximum and the convection reversal. However, for the positive IMF By, the maximum of the upward field-aligned current was
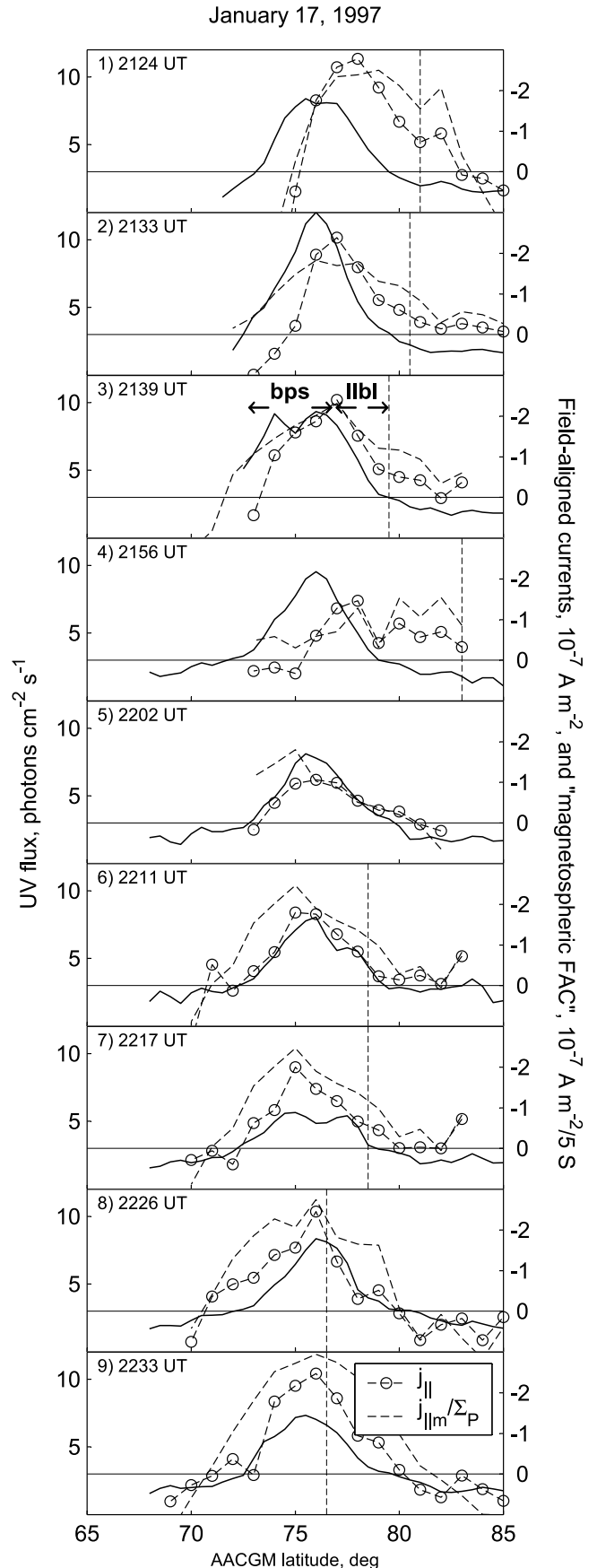
Figure 9. (opposite) The same as Figure 8, but for the event of 17 January. The sequence corresponds to the IMF By transition from positive values (top panels) to negative values (bottom panels). Times of UV images are indicated in the plots. Magnetospheric regions (BPS and LLBL) in panel 3 were identified from the DMSP F13 satellite.

January 17, 1997

poleward of the auroral maximum and it was associated with the poleward edge of the auroral oval.

[42] Poleward of the auroral oval, the field-aligned currents tend to be upward for IMF By > 0 (Figure 9, panels 1–4). For IMF By < 0, downward FACs were observed poleward of the auroral oval (panels 8–9 in Figure 9, and case of 22 February in Figure 8).

[43] According to *Sofko et al.* [1995], the field-aligned current (4) may be represented as a sum of two parts, the "magnetospheric component" $j_{\|m}$ of the FAC

$$j_{\|m}/\Sigma_P = \frac{\partial E_x}{\partial x}, \tag{10}$$

and the "ionospheric component" given by

$$j_{\|i} = E_x \frac{\partial}{\partial x}\Sigma_P - E_y \frac{\partial}{\partial x}\Sigma_H. \tag{11}$$

Following *Sofko et al.* [1995], we shall consider the "magnetospheric" FAC in terms of vorticity, $j_{\|m}/\Sigma_P$, which value does not depend on the ionospheric conductivity. Thin dash lines in Figures 8 and 9 show the "magnetospheric" FAC, which corresponds to the constant Pedersen conductance indicated in the figures (this conductance is used as a scaling factor to match the total FAC). On 17 January (Figure 9), the "magnetospheric" FAC $j_{\|m}/\Sigma_P$ demonstrated similar behavior versus time and latitude as the total field-aligned currents. In three cases in Figure 8, peaks of the "magnetospheric" and total FACs are coinciding or located very close to each other. Equatorward of the auroral maximum, the behavior of the "magnetospheric" FAC $j_{\|m}/\Sigma_P$ versus latitude is similar to one of the total field-aligned currents. However, a difference between them occurs at the poleward edge of the auroral oval, that indicates a downward FAC associated with sharp conductivity gradient.

[44] Indeed, the "magnetospheric" FAC accounts for both the electric field from magnetospheric sources and the polarization electric field originating from the gradient of the ionospheric conductivity as well. The vorticity is calculated independently of the assumptions on the ionospheric conductivity so the "magnetospheric" FAC $j_{\|m}/\Sigma_P$ represents "pure" convection effects derived from the SuperDARN observations that do not depend on the Polar UVI data. The calculated total FAC depends on both the ionospheric conductivity (UVI intensity) and the electric field (SuperDARN). However, the location and temporal variations of the FAC maximum are governed mainly by the "magnetospheric" component (as seen in Figures 8, 9, and also in Figure 10). Thus, in fact one compares the locations and temporal behaviors of the two independently measured characteristics, which are the peak of auroral intensity and the maximum of "magnetospheric" FAC $j_{\|m}/\Sigma_P$.

[45] The main results of this section may be summarized as follows. The postnoon (14–17 MLT) auroral oval is associated with the large-scale upward field-aligned current of the order of 6×10^{-7} A m^{-2} in magnitude. For negative IMF By, maximum of the auroral intensity coincides in latitude with both the maximum of upward field-aligned current and the convection reversal. However, for positive
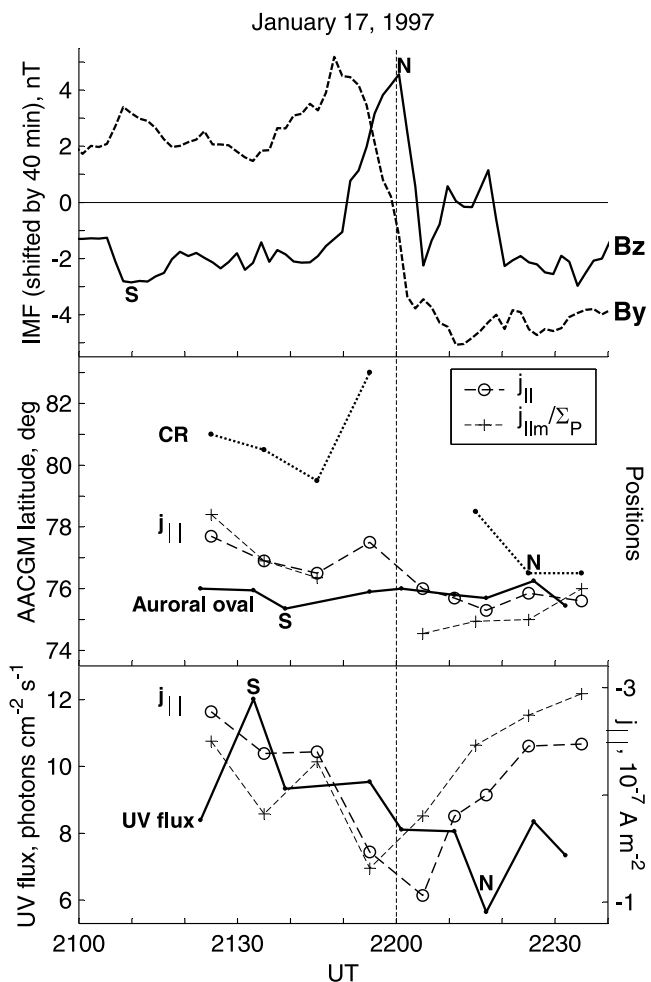

Figure 10. Temporal variations of various parameters during the IMF By transition event of 17 January. Top panels show the IMF By and Bz components time-shifted to get a correspondence with the convection patterns. Middle panel shows latitudinal positions of the convection reversal (dotted line), maximums of FAC (dashed lines with open circles and crosses for total and "magnetospheric" FAC $j_{\|m}/\Sigma_P$, respectively), and UV intensity (solid line) versus time. Bottom panel gives magnitudes of the FAC and UV intensity maximums versus time (the same line types as in the middle panel). The "magnetospheric component" of FAC was computed for the Pedersen conductance of 5 S.

IMF By, the maximum of the upward FAC is shifted to the poleward edge of the auroral oval.

6. IMF Change

[46] In this section we analyze in detail variations in convection, FAC, and auroral luminosity that occurred during the interval of the IMF By change, 17 January, 2120–2240 UT. Latitudinal distributions of these parameters with about 10-min resolution are presented in Figure 9. To make the presentation clearer, we have determined latitudinal positions of the FAC and luminosity maxima as mean latitudes between the two points obtained by crossing the data points with a line at a level of 0.7 from the

maximum value. These latitudinal positions of maxima versus time are presented in the middle panel of Figure 10 together with the latitudes of the convection reversal. The bottom panel shows magnitudes of the FAC and UV intensity maxima versus time. Figure 10 also shows positions and magnitudes of the "magnetospheric" FACs $j_{\|m}/\Sigma_P$ (these are about the same as the total field-aligned currents, as seen in Figure 9). The top panels in Figure 10 show the IMF By and Bz components, time-shifted to obtain a correspondence with the convection patterns.

6.1. Response to IMF By

[47] The IMF data (Figure 10) indicate rotation of the magnetic field vector in the $Y-Z$ plane from positive By to negative one through positive Bz at about 2200 UT. From the middle panel of Figure 10 one can see that maximum of the auroral luminosity did not change much in its position and was at about $76 \pm 0.5°$ MLAT both before and after the IMF By turning. At the same time, the position of the convection reversal has changed considerably from $80-81°$ to $76.5°$ MLAT, and the maximum of FAC moved noticeably from $77°$ to about $75.5°$ MLAT. Thus, by 2230 UT (when IMF By became negative) both FAC maximum and CR came close (within $1°$ in latitude) to the auroral maximum.

6.2. Response to IMF Bz

[48] The IMF vector rotation in the $Y-Z$ plane from positive By to negative one was associated with a short, of the order of $15-20$ min, positive (northward) deflection in the IMF Bz component at about 2200 UT (indicated by letter N). Also we would like to mention the IMF Bz negative deflection from -1.5 to -3 (southward) at 2110 UT (indicated by letter S). It has earlier been known that southward IMF turnings were followed by equatorward motion of the postnoon auroral oval [e.g., *Kozlovsky and Kangas*, 2001]. On the other hand, northward IMF Bz turnings have been found to be associated with poleward expansions of the postnoon auroral oval [*Ohtani et al.*, 1997]. Thus, a correspondence should be expected between IMF Bz and latitudinal location of the auroral oval (solid line in middle panel of Figure 10). So the equatorward shift of the auroral maximum at about 2140 UT (indicated by S) is probably related to the IMF Bz deflection from -1.5 to -3 at 2110 UT (30 min earlier), and the positive Bz deflection at 2200 UT (indicated by S) would result in the poleward motion of the auroral oval observed at 2225 UT (25 min later). The variations in location of the auroral maximum are of the order of 50 km, which corresponds to the UVI resolution (the wobbling effect did not affect the latitudinal location in the postnoon, as was shown in section 3). The observed time lag behind the ionospheric convection (30 and 25 min) agrees with earlier result of *Kozlovsky and Kangas* [2001] who reported that changes in latitudinal location of the postnoon auroral oval lag behind IMF Bz variations in the subsolar point by $20-35$ min.

[49] It is known that the brightness of auroral forms in the postnoon tends to increase with the IMF Bz decreasing from positive (northward) to negative (southward) values [e.g., *Meng and Lundin*, 1986; *Kozlovsky and Kangas*, 2001]. This effect is well seen in the auroral intensity presented in the bottom panel of Figure 10 where the increase and decrease of the UV flux (indicated by letters S and N, respectively) follow the IMF Bz deflections indicated by the corresponding letters. Thus, both the auroral brightness and location of the auroral oval responded to IMF Bz variations in the way that would be expected from previous studies.

[50] The behavior of the field-aligned current intensity also agrees with the earlier results that suggested that the region 2 FAC density is directly proportional to increases of the IMF in the "$-z$" (southward) direction [*Potemra*, 1994]. The bottom panel in Figure 10 shows that the IMF Bz deflection to positive was associated with a decrease in the field-aligned current density. The peak FAC intensity decreased from 0.3 to 0.1 10^{-6} A m^{-2} at 2205 UT, which corresponds to the IMF Bz deflection to positive values. However, a corresponding decrease in the auroral luminosity (from $10-12$ to 6 photons cm^{-2} s^{-1}) was detected at 2217 UT, i.e., 12 min later. The time uncertainty of the auroral intensity minimum (± 4 min) results from the 8-min interval between the UVI frames whereas the FAC time uncertainty (± 5 min) is due to 10-min SuperDARN integration time, so the uncertainty in the lag time can be estimated as ± 7. "Magnetospheric" FAC has a minimum at 2155, i.e., 22 ± 7 min earlier than the auroral intensity minimum.

[51] Thus, the main result of this section is that the IMF Bz positive deflection was followed by a decrease in both field-aligned current intensity and auroral luminosity in the postnoon auroral oval However the decrease in auroral luminosity lags behind the FAC decrease by 12 ± 7 min.

7.   Summary and Discussion

[52] We enumerate below all of the results of our study. Some of them were known earlier and/or agree with the results of the earlier papers we refer to.

1. The postnoon auroral oval was mostly associated with particle precipitation from the BPS (section 3). Such an observation was reported in earlier papers [e.g., *Ohtani et al.*, 1995; *Liou et al.*, 1999; *Starkov et al.*, 2002].

2. The postnoon auroral oval was associated with the upward field-aligned current of the order of 6×10^{-7} A m^{-2} in magnitude, and downward field-aligned current was observed equatorward of the auroral oval. Poleward of the auroral oval, the field-aligned currents tend to be upward for IMF By > 0. For IMF By < 0, downward FACs were observed poleward of the auroral oval (section 5). These observations agree with many previous studies mentioned in Introduction. Notably, we refer to *Watanabe et al.* [1996, 1998] who investigated a large-scale FAC distribution as depended on IMF By, and obtained that Region 1 (R1) postnoon FACs are associated with BPS (or LLBL in the earlier afternoon).

3. For negative IMF By, the maximum of the auroral intensity coincides in latitude with the maximum of the upward field-aligned current. However, for positive IMF By, the maximum of the upward FAC was shifted to the poleward edge of the auroral oval (sections 5 and 6).

4. For negative IMF By, the convection reversal (CR) was colocated with the maximum of auroral luminosity, but during positive IMF By, the convection reversal was poleward of the auroral oval up to several degrees in latitude (section 4).

5. In response to IMF By turning from positive to negative, the maximum of the auroral luminosity did not change its position noticeably, but the position of the convection reversal changed considerably, from 80°–81° to about 76° MLAT, and the maximum of FAC moved from 77°–78° to about 76° MLAT (section 6.1).

6. The equatorward (poleward) shifts of the auroral oval followed 25–30 min after IMF Bz positive (negative) deflections arrived to the polar cap ionosphere (section 6.2). This agrees with the earlier result of *Kozlovsky and Kangas* [2001] where this phenomenon was discussed in more detail.

7. The IMF Bz positive deflection was followed by a decrease in both field-aligned current intensity and auroral luminosity. However, the decrease in the auroral luminosity lags behind the FAC decrease by 12 ± 7 min. The "magnetospheric" FAC minimum occurred 22 ± 7 min before the auroral intensity minimum (section 6.2).

[53] The most important and novel results are 3 and 7 that concern the relationship of auroral luminosity and FACs, and 4 and 5 concerning the CR position with respect to the auroral oval. These two issues, the relations of the postnoon auroral luminosity with FAC and CR, are further discussed in the following.

7.1. Relation of Aurora and FAC

[54] First of all, we shall suggest an explanation why the field-aligned currents turned out to be associated with particle precipitation in case of By < 0 and to be separated of precipitation in case of By > 0.

[55] In section 1.1 above we suggested three possible source mechanisms of the field-aligned currents which can operate in the postnoon auroral oval, namely the solar wind merging effects for various IMF Bz and By components, the viscous solar wind–magnetosphere interaction, and drift currents produced in plasma pressure gradient regions. As many results show, plasma pressure gradients are the most effective source of field-aligned currents in the low-latitude boundary layer as well as at the boundaries of the plasma sheet (e.g., in the BPS) [e.g., *Troshichev*, 1982; *Yamamoto et al.*, 1996; *Shiokawa et al.*, 1998]. The estimations made on the basis of plasma measurements in LLBL showed that the currents caused by plasma pressure gradients in LLBL are a factor of hundred higher than the currents resulted from the viscous interaction [*Troshichev*, 1982]. *Watanabe et al.* [1996, 1998] have shown that R1 postnoon FACs are associated with BPS or LLBL, whose results also support the role of the plasma pressure gradients. Thus, the plasma pressure gradient can be considered as the main mechanism for the postnoon R1 FAC. These field-aligned currents are given by the formula [*Vasyliunas*, 1970]:

$$j_{\parallel \nabla P} = \frac{1}{2}(\mathbf{e}_z \cdot (\nabla W \times \nabla P)), \tag{12}$$

where W is a volume of magnetic flux tube with unit magnetic flux, P is the plasma pressure, and $\mathbf{e}_z$ is the unit vector directed along the magnetic field.

[56] Large-scale upward FAC is carried by downward electron flux and provides favorable conditions for auroras. However, the intensity of the auroral oval depends mainly on small-scale bright auroral forms (discrete auroras), which are due to instabilities in the magnetosphere–ionosphere system. If the field-aligned current determined by equation (12) is nonzero (i.e., if $\nabla P \times \nabla W \neq 0$), the plasma boundary is unstable with respect to the interchange instability [e.g., *Volkov and Maltsev*, 1986; *Kozlovsky and Lyatsky*, 1994; *Lyatsky and Sibeck*, 1997]. In some papers terms "flute" [e.g., *Pochotelov et al.*, 1980] or "ballooning" [e.g., *Miura et al*, 1989] are used for such kind of instability (terms "slot" and "exchange" appeared in [*Volkov and Maltsev*, 1986] because of wrong translation from Russian). This is a certain analog to the Rayleigh–Taylor instability. The interchange instability develops at the growth rate given by

$$\Gamma = \frac{\left| j_{\parallel \nabla P} \right|}{2\Sigma_P B_i} \tan\left(\frac{\alpha}{2}\right), \tag{13}$$

where Bi is the ionospheric magnetic field magnitude, and α is the angle between two gradients, $\nabla(PW^\gamma)$ and $\nabla(P^{-\beta/2}W)$ [*Volkov and Maltsev*, 1986]. Here γ and β are the adiabatic exponent and the gas-to-magnetic pressure ratio, respectively. The angle α is nonzero in all the cases when $\nabla P \times \nabla W \neq 0$. The pressure gradient existing in BPS gains a normal component to ∇W due to sunward magnetospheric convection [e.g., *Yamamoto et al.*, 1996], which leads to both the FAC (12) and the instability (13). The instability splits the plasma boundary into small-scale tongue-like structures, which give rise to the discrete auroras forming the bright auroral oval. Thus, the postnoon auroral oval relates to BPS and is colocated with the main part of R1 FAC given by (12).

[57] However, the field-aligned current distribution can be essentially affected by ionospheric conductivity gradients [e.g., *Bristow and Lummerzheim*, 2001]. Due to this effect, additional field-aligned currents arise in the regions of conductivity gradients and flow between the conjugate hemispheres. Such currents were studied in detail theoretically by *Benkevich et al.* [2000] who have shown that the magnitude of the interhemispheric currents can be comparable with that of the R1 field-aligned currents. In the winter ionosphere, the direction of the interhemispheric currents, $j_{\parallel \nabla \Sigma}$, at the edges of the postnoon auroral oval can be estimated from the two-hemisphere current continuity equation [*Benkevich et al.*, 2000] as

$$j_{\parallel \nabla \Sigma} \propto \mathbf{E} \cdot \nabla \Sigma_P. \tag{14}$$

Here we consider the conjugate summer ionosphere as highly and homogeneously conducting (comparing to the northern one) and neglect the Hall current across the auroral oval, which is a simplification but relevant and applies to the case of 17 January. Equation (14) indicates that the interhemispheric currents are positive (downward) or negative (upward) if the conductivity gradient is along or against the electric field, respectively. In the postnoon ionosphere, the electric field points toward the convection reversal. In the cases when the IMF By < 0 (e.g., Figure 9, panels 8 and 9), the convection reversal is in the center of the auroral oval, so the interhemispheric currents are downward at both boundaries of the auroral oval that does not affect the position of the total FAC given by the sum of equations (12) and (14). In the case when the IMF By > 0

(Figure 9, panels 1–3), the electric field is northward, so the interhemispheric currents are upward at the poleward edge of the auroral oval. The maximum of the total FAC given by the sum of equations (12) and (14) may not coincide with the auroral oval because the auroral luminosity is mostly associated with the current equation (12) and the plasma pressure gradient in BPS.

[58] As was mentioned above, the sunward magnetospheric convection governs both the FAC (equation 12) and the interchange instability (equation 13). In response to IMF Bz northward turning, the sunward convection decreases followed some later by the decrease of the pressure gradient normal component to ∇W. Hence, the FAC (equation 12) decreases and the interchange instability (equation 13) calms down. However, the already existing magnetospheric inhomogeneities and hence, the corresponding auroras need some time to dissipate. Our observations suggest 22 and 12 min lag times of the auroral processes after the electric field ("magnetospheric" FAC) and field-aligned currents, respectively. This result agrees with the earlier observations of *Ohtani et al.* [1997] who reported that the dayside auroral process has a finite decay constant, which was inferred to be at least 10 min. In fact, the small-scale magnetospheric inhomogeneities discussed above are the magnetic flux tubes containing the hot plasma. Such configurations are unstable, and the interchange instability is the strongest mechanism to destroy them [e.g., *Kadomtsev*, 1988]. The characteristic time of the interchange instability in the magnetosphere is of the order of 10 min [e.g., *Volkov and Maltsev*, 1986; *Kozlovsky and Lyatsky*, 1994]. For this reason, the auroral intensity should lag behind the FAC intensity changes by about 10 min.

[59] This time lag and latitudinal distance between the auroras and FAC are probably the most interesting results of our study. For explanation of these effects we considered the interchange instability, but certainly additional studies should be done to understand the relation between the field-aligned currents and auroras in the postnoon sector. These future studies should include also small-scale observations, which could not be done with the instruments used in present paper.

7.2. Location of the Convection Reversal

[60] In this section we discuss the finding that for negative IMF By, the convection reversal at 14–17 MLT was located inside the auroral oval close to the maximum of auroral luminosity, whereas during positive IMF By the convection reversal was poleward of the auroral oval.

[61] First, this result agrees with the earlier studies mentioned in section 1.2. *Moen et al.* [1994] reported that the postnoon aurora was equatorward of the convection reversal boundary, whose observation was made during IMF By > 0. On the other hand, *Kozlovsky and Kangas* [2001] presented four cases that were observed during IMF By < 0 and showed that the CR location occurred inside the auroral oval.

[62] Second, many researchers observed the By-dependence of the CR position. For example, *Rash et al.* [1999] found a significant correlation between IMF By and the latitude of CR in the morning sector. Indeed, the convection patterns observed during the IMF By change on 17 January agree with many other papers where effects of IMF in high-

latitude convection have been studied with SuperDARN radar data [e.g., *Greenwald et al.*, 1990; *Ruohoniemi and Greenwald*, 1995, 1996; *Amm et al.*, 1999]. The change in CR latitudinal position following after IMF By turning was observed by *Amm et al.* [1999], but these authors did not study the location of the auroral oval at the same time. On a statistical basis, *Ruohoniemi and Greenwald* [1995, 1996] obtained that negative (positive) IMF By conditions cause a crescent-shaped convection cell in the dusk (dawn) sector. The center of the dusk cell (and the CR) moves equatorward as the cell becomes more crescent-shaped caused by changes in the IMF By from positive to negative, which also agrees well with the case presented in Figure 1.

[63] A theoretical explanation for the IMF By-depended plasma flows on the dayside magnetosphere has been given by *Burch et al.* [1985] and *Reiff et al.* [1985]. This model suggests that the IMF By component governs plasma flow in lobe cells and positions of the lobe cells. In the northern polar cap, the plasma flows are westward (eastward) and the cells are shifted toward the dusk (dawn) for positive (negative) IMF By. In the southern polar cap, the flow direction and the cell position are opposite. The IMF By-associated plasma flows are to be confined in the open polar cap. Due to the high field-aligned conductivity, the contra-directed plasma flows in the conjugate hemispheres cannot coexist (in a steady state). To satisfy this condition, the additional convection reversal was assumed just at the open-closed boundary in the postnoon for IMF > 0 (in the northern hemisphere), although its existence had not been confirmed [*Burch et al.*, 1985]. Later observations [e.g., *Ruohoniemi and Greenwald*, 1996] have not indicated such a convection reversal, and our data do not show it. Moreover, the case of 17 January shows that the IMF By-associated convection changes occurred in the closed magnetosphere (in the BPS), which resulted in changes of the CR position with respect to the auroral oval. To illustrate this feature, Figure 11 shows the differential convection pattern obtained by subtracting the convection diagram *f* in Figure 1 (IMF By ≈ −5) from diagram *b* (IMF By ≈ +2). Other interplanetary parameters for these diagrams (SW pressure, IMF Bz and Bx) do not differ much, so the differential plasma flow in Figure 11 should be attributed mainly to the IMF By turning. A cross with open circle indicates downward FAC in the polar cap and a dot with open circle shows the upward FAC equatorward of the auroral oval, whose currents appeared following the IMF changing.

[64] Thus, Figure 11 demonstrates that the IMF By-related electric field can penetrate into the closed magnetosphere and produce convection changes in the region of the postnoon auroral oval. This conclusion can find a significant support in some observations reported earlier [*Ruohoniemi and Greenwald*, 1995; *Milan et al.*, 2001; *Khan and Cowley*, 2001]. However, the problem of IMF By-related convection flow in closed magnetosphere has not been resolved yet.

[65] *Khan and Cowley* [2001] have analyzed a database of 300 hours of plasma velocity measurements obtained by the EISCAT UHF radar system at Tromsø (66.3° magnetic latitude). They found that significant flow variations with IMF By occur, predominantly in the midnight sector (2100–0300 MLT), but also in predusk (1600–1700
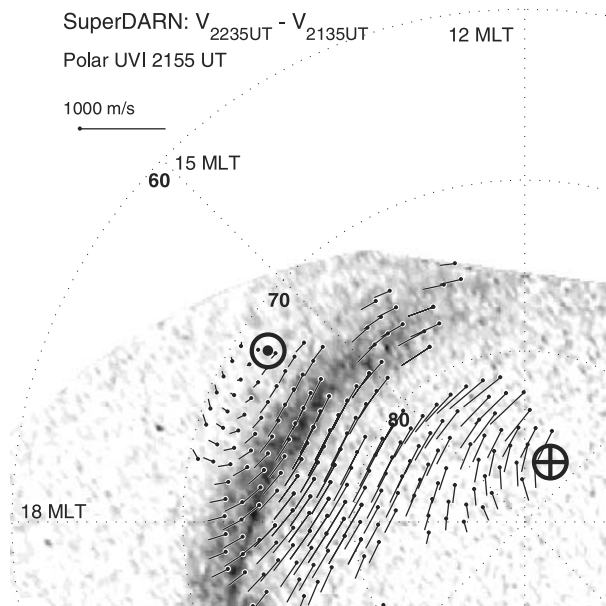
SuperDARN: V$_{2235UT}$ - V$_{2135UT}$ 12 MLT

Polar UVI 2155 UT

1000 m/s

15 MLT

60

70

80

18 MLT

Figure 11. Differential plasma flow associated with IMF By changing. The differential convection pattern was obtained by subtracting of convection diagram *f* in Figure 1 (IMF By ≈ −5) from diagram *b* (IMF By ≈ +2). A cross with open circle indicates downward FAC in the polar cap and a dot with open circle show the upward FAC equatorward of the auroral oval.

MLT) sector. They investigated whether these IMF By-dependent flows can be accounted by a model in which the equatorial flow in the inner magnetosphere is independent of IMF By, but where distortions of the magnetospheric magnetic field associated with a "penetrating" component of the IMF By field changes the mapping of the field to the ionosphere, and hence the ionospheric flow. The model results have been found to account well for the observed IMF By-related flow perturbations in the midnight sector. However, the model does not account for the effects observed in the predusk sector.

[66] *Ruohoniemi and Greenwald* [1995] performed a statistical analysis of observations made with the Goose Bay SuperDARN radar and obtained strong IMF By and seasonal effects in the convection of nightside ionospheric plasma. It is important that the seasonal dependence resembled the IMF By effect with summer showing more By > 0 character. *Milan et al.* [2001] obtained that the influence of the IMF By on the convection depends on season. The seasonal effects reported by *Ruohoniemi and Greenwald* [1995] and *Milan et al.* [2001] allow us to suppose that the IMF By-related convection and FAC disturbances in closed magnetosphere may be explained in the framework of a model including a seasonal interhemispheric asymmetry (ionospheric conductivity and maybe the Earth's dipole angle).

[67] Finally, we shall explain the observed CR location with respect to the auroral oval. As was discussed above, the postnoon aurora is related to BPS and, hence, depends mainly on the plasma sheet position. The plasma sheet position does not show a dependence on the IMF By. However, the plasma flow does change with the IMF By.

When IMF By < 0, the By-related convection focus is shifted to dawn side. Hence, the location of the postnoon convection reversal mainly depends on the pressure gradient and other sources like IMF Bz and viscous interaction on the magnetopause, which gives the CR location in the auroral oval. If IMF By is positive, an additional westward plasma flow appears in the northern polar ionosphere (opposite to one shown in Figure 11). This By-associated plasma flow is most intense on the dusk side and shifts the postnoon convection reversal poleward. Thus, the westward plasma flow associated with IMF By > 0 can explain the location of CR with respect to the auroral oval. However, the problem is how to explain the IMF By-associated plasma flow on closed magnetic field lines. Most probably, this problem can be solved by taking into account the different conductivity distributions in the opposite hemispheres.

8. Conclusion

[68] The ultraviolet imager onboard Polar satellite and SuperDARN radar network allowed us to observe the auroral oval together with the ionospheric convection. The following observations made in the postnoon (14–17 MLT) auroral oval may be mentioned as the most important ones:

1. The IMF By component controls the location of the convection reversal with respect to the auroral oval. For negative IMF By, the convection reversal is located inside the auroral oval close to the maximum of auroral luminosity while for positive IMF By, the convection reversal is located poleward of the auroral oval (up to several degrees in latitude).

2. In response to IMF By turning from positive to negative values, the maximum of the auroral luminosity does not change its position staying at ∼76° MLAT whereas the convection reversal moves considerably from 80°–81° to about 75°–76° MLAT.

3. For negative IMF By, the maximum of the auroral intensity coincides in latitude with the maximum of upward field-aligned current, however for positive IMF By maximum of the upward FAC was shifted to the poleward edge of the auroral oval.

4. The IMF Bz positive deflection is accompanied by a decrease in the field-aligned current intensity. The corresponding decrease in the auroral luminosity lags behind the field-aligned current decrease by 12 min.

[69] Results 1 and 2 allow us to suggest that the IMF By-related electric field can penetrate into the closed magnetosphere and produce convection changes in the region of the postnoon auroral oval. Results 3 and 4 (relations between the auroral oval and FAC) allow us to propose the interchange instability as a promising mechanism for the postnoon auroras.

References

Amm, O., M. J. Engebretson, R. A. Greenwald, H. Luhr, and T. Moretto, Direct determination of IMF By related cusp current system, using Super-DARN radar and multiple ground magnetometer data: A link to theory on cusp current origin, *J. Geophys. Res.*, *104*, 17,187–17,198, 1999.

Axford, W. I., and C. O. Hines, A unifying theory of high-latitude geophysical phenomena and geomagnetic storm, *Can. J. Phys.*, *39*, 1433–1464, 1961.

Baker, K. B., and S. Wing, A new magnetic coordinate system for conjugate studies at high latitudes, *J. Geophys. Res.*, *94*, 9139–9143, 1989.

Benkevich, L., W. Lyatsky, and L. L. Cogger, Field-aligned currents between conjugate hemispheres, *J. Geophys. Res.*, *105*, 27,727–27,738, 2000.

Bristow, W. A., and D. Lummerzheim, Determination of field-aligned currents using the Super Dual Auroral Radar Network and the UVI ultraviolet imager, *J. Geophys. Res.*, *106*, 18,577–18,587, 2001.

Burch, J. L., P. H. Reiff, J. D. Menietti, R. A. Heelis, W. B. Hanson, S. D. Shawhan, E. G. Shelley, M. Sugiura, D. R. Weimer, and J. D. Winningham, IMF By-dependent plasma flow and Birkeland currents in the dayside magnetosphere, 1, Dynamics Explorer observations, *J. Geophys. Res.*, *90*, 1577–1593, 1985.

Bythrow, P. F., R. A. Heelis, W. B. Hanson, R. A. Power, and R. A. Hoffman, Observational evidence for a boundary layer source of dayside Region 1 field-aligned currents, *J. Geophys. Res.*, *86*, 5577–5589, 1981.

Bythrow, P. F., B. J. Anderson, T. A. Potemra, L. J. Zanetti, J. D. Winningham, and D. L. Chenette, Filamentary current structures in the postnoon sector: Observations from UARS, *J. Geophys. Res.*, *99*, 14,917–14,929, 1994.

Cogger, L. L., J. S. Murphree, S. Ismail, and C. D. Anger, Characteristics of dayside 5577 A and 3914 A aurora, *Geophys. Res. Lett.*, *4*, 413–416, 1977.

Dungey, J. W., Interplanetary magnetic field and the auroral zones, *Phys. Rev. Lett.*, *6*, 47–48, 1961.

Evans, D. S., The characteristics of a persistent auroral arc at high latitude in the 1400 MLT sector, in *The Polar Cusp: Proceedings of the Advanced Research Workshop on the Morphology and Dynamics of the Polar Cusp, Lillehammer, Norway, 7–12 May 1984*, pp. 99–109, D. Reidel, Norwell, Mass., 1985.

Fairfield D. H., Average and unusual location of the Earth's magnetopause and bow shock, *J. Geophys. Res.*, *76*, 6700–6716, 1971.

Germany, G. A., J. F. Spann, G. K. Parks, M. J. Brittnacher, R. Elsen, L. Chen, D. Lummerzheim, and M. H. Rees, Auroral Observations from the POLAR Ultraviolet Imager (UVI), in *Geospace Mass and Energy Flow: Results from the International Solar-Terrestrial Phsics Program*, edited by J. Horwitz, D. Gallagher, and W. Peterson, pp. 149–160, AGU, Washington, D. C., 1998.

Greenwald, R. A., K. B. Baker, J. M. Ruohoniemi, J. R. Dudeney, M. Pinnock, N. Mattin, J. M. Leonard, and R. P. Lepping, Simultaneous conjugate observations of dynamic variations in high-latitude dayside convection due to changes in IMF By, *J. Geophys. Res.*, *95*, 8057–8072, 1990.

Greenwald, R. A., et al., DARN/SuperDARN: A global view of high-latitude convection, *Space Sci. Rev.*, *71*, 763–796, 1995.

Gustafsson, G., N. E. Papitashvili, and V. O. Papitashvili, A revised corrected geomagnetic coordinate system for Epochs 1985 and 1990, *J. Atmos. Terr. Phys.*, *54*, 1609–1631, 1992.

Iijima, T., and T. A. Potemra, The amplitude distribution of field-aligned currents at northern high latitudes observed by Triad, *J. Geophys. Res.*, *81*, 2165–2174, 1976a.

Iijima, T., and T. A. Potemra, Field-aligned currents in the dayside cusp observed by Triad, *J. Geophys. Res.*, *81*, 5971–5979, 1976b.

Iijima, T., T. A. Potemra, and L. J. Zanetti, Contribution of pressure gradients to the generation of dawnside Region 1 and Region 2 currents, *J. Geophys. Res.*, *102*, 27,069–27,082, 1997.

Kadomtsev B. B., *Collective Phenomena in Plasmas* (in Russian), p. 304, Nauka, Moscow, 1988.

Khan, H., and S. W. H. Cowley, Effect of the IMF By component on the ionospheric flow overhead at EISCAT: Observations and theory, *Ann. Geophys.*, *18*, 1503–1522, 2001.

Kozlovsky, A., and J. Kangas, Characteristics of the post-noon auroras inferred from EISCAT radar measurements, *J. Geophys. Res.*, *106*, 1817–1834, 2001.

Kozlovsky, A. E., and W. B. Lyatsky, Instability of the magnetosphere–ionosphere convection and formation of auroral arcs, *Ann. Geophys.*, *12*, 636–641, 1994.

Kustov, A. V., W. B. Lyatsky, and G. J. Sofko, SuperDARN observations of near-noon plasma convection at small interplanetary magnetic field Bz and By, *J. Geophys. Res.*, *103*, 4041–4050, 1998.

Liou, K., P. T. Newell, C.-J. Meng, M. Brittnacher, and G. Parks, Synoptic auroral distribution: A survey using Polar ultraviolet imagery, *J. Geophys. Res.*, *102*, 27,197–27,205, 1997.

Liou, K., P. T. Newell, C.-J. Meng, M. Brittnacher, and G. Parks, Characteristics of the solar wind controlled auroral emissions, *J. Geophys. Res.*, *103*, 17,543–17,557, 1998.

Liou, K., P. T. Newell, C.-I. Meng, T. Sotirelis, M. Brittnacher, and G. Parks, Source region of 1500 MLT auroral bright spots: Simultaneous Polar UV-images and DMSP particle data, *J. Geophys. Res.*, *104*, 24,587–24,602, 1999.

Lockwood, M., P. E. Sandholt, S. W. H. Cowley, and T. Oguti, Interplanetary magnetic field control of dayside auroral activity and the transfer of momentum across the dayside magnetopause, *Planet. Space Sci.*, *37*, 1347–1365, 1989.

Lu, G., L. R. Lyons, P. H. Reiff, W. F. Denig, O. de la Beaujardiere, H. W. Kroehl, P. T. Newell, F. J. Rich, H. Opgenoorth, and M. A. L. Persson, Characteristics of ionospheric convection and field-aligned current in the dayside cusp region, *J. Geophys. Res.*, *100*, 11,845–11,861, 1995.

Lui, A. T. Y., D. Venkatesan, and J. S. Murphree, Auroral bright spots on the dayside oval, *J. Geophys. Res.*, *94*, 5515–5522, 1989.

Lyatsky, W. B., and D. G. Sibeck, Central plasma sheet disruption and the formation of dayside poleward moving auroral events, *J. Geophys. Res.*, *102*, 17,625–17,630, 1997.

Meng, C.-I., and R. Lundin, Auroral morphology of the midday oval, *J. Geophys. Res.*, *91*, 1572–1584, 1986.

Milan, S. E., L. J. Baddeley, M. Lester, and N. Sato, A seasonal variation in the convection response to IMF orientation, *Geophys. Res. Lett.*, *28*, 471–474, 2001.

Miura, A., S. Ohtani, and T. Tamao, Ballooning instability and structure of diamagnetic hydromagnetic waves in a model magnetosphere, *J. Geophys. Res.*, *94*, 15,231–15,242, 1989.

Moen, J., P. E. Sandholt, M. Lockwood, A. Egeland, and K. Fukui, Multiple, discrete arcs on sunward convecting field lines in the 14–15 MLT region, *J. Geophys. Res.*, *99*, 6113–6123, 1994.

Murphree, J. S., L. L. Cogger, and C. D. Anger, Characteristics of the instantaneous auroral oval in the 1200–1800 MLT sector, *J. Geophys. Res.*, *86*, 7657–7668, 1981.

Newell P. T., W. J. Burke, E. R. Sanchez, C.-I. Meng, M. E. Greenspan, and C. R. Clauer, The low latitude boundary layer and the boundary plasma sheet at low altitude: Prenoon precipitation regions and convection reversal boundaries, *J. Geophys. Res.*, *96*, 21,013–21,024, 1991.

Newell, P. T., K. Liou, T. Sotirelis, and C.-I. Meng, Auroral precipitation power during substorms: A polar UV Imager-based superposed epoch analysis, *J. Geophys. Res.*, *106*, 28,885–28,896, 2001.

Ohtani, S., T. A. Potemra, P. T. Newell, L. J. Zanetti, T. Iijima, M. Watanabe, M. Yamauchi, R. D. Elphinstone, O. de La Beauijardie, and L. G. Blomberg, Simultaneous prenoon and postnoon observations of three field-aligned current systems from Viking and DMSP-F7, *J. Geophys. Res.*, *100*, 119–136, 1995.

Ohtani, S., R. D. Elphinstone, O. A. Troshichev, M. Yamauchi, L. Blomberg, L. J. Zanetti, and T. A. Potemra, Response of the dayside auroral and electrodynamic processes to variations in the interplanetary magnetic field, *J. Geophys. Res.*, *102*, 22,247–22,260, 1997.

Pochotelov, O. A., A. M. Buloshnikov, and V. A. Pilipenko, Hydromagnetic stability of the outer boundary of the captured radiation, *Geomagn. Aeron., Engl. Transl.*, *20*, 289–292, 1980.

Potemra T. A., Sources of large-scale Birkeland currents, in *Physical Signatures of Magnetospheric Boundary Layer Processes*, edited by J. A. Holtet and A. Egeland, pp. 3–27, Kluwer Acad., Norwell, Mass., 1994.

Rash, J. P. S., A. S. Rodger, and M. Pinnock, HF radar observations of the high-latitude ionospheric convection pattern in the morning sector for northward IMF and motion of the convection reversal boundary, *J. Geophys. Res.*, *104*, 14,847–14,866, 1999.

Reiff, P. H., and J. L. Burch, IMF By-dependent plasma flow and Birkeland currents in the dayside magnetosphere, 2, A global model for northward and southward IMF, *J. Geophys. Res.*, *90*, 1595–1609, 1985.

Ridley, A. J., Estimations of the uncertainty in timing the relationship between magnetospheric and solar wind processes, *J. Atmos. Sol. Terr. Phys.*, *62*, 757–771, 2000.

Robinson, R., M. R. R. Vondrak, K. Miller, T. Dabbs, and D. Hardy, On calculating ionospheric conductances from the flux and energy of precipitating electrons, *J. Geophys. Res.*, *92*, 2565–2569, 1987.

Ruohoniemi, J. M., and K. B. Baker, Large-scale imaging of high-latitude convection with Super Dual Auroral Radar Network HF radar observations, *J. Geophys. Res.*, *103*, 20,797–20,812, 1998.

Ruohoniemi, J. M., and R. A. Greenwald, Observations of IMF and seasonal effects in high-latitude convection, *Geophys. Res. Lett.*, *22*, 1121–1124, 1995.

Ruohoniemi, J. M., and R. A. Greenwald, Statistical patterns of high-latitude convection obtained from Goose Bay HF radar observations, *J. Geophys. Res.*, *101*, 21,743–21,764, 1996.

Ruohoniemi, J. M., and R. A. Greenwald, The response of high-latitude convection to a sudden southward IMF turning, *Geophys. Res. Lett.*, *25*, 2913–2916, 1998.

Shepherd, G. G., F. W. Thirkettle, and C. D. Anger, Topside optical view of the dayside cleft aurora, *Planet. Space Sci.*, *24*, 937–944, 1976.

Shiokawa, K., G. Haerendel, and W. Baumjohann, Azimuthal pressure gradient as driving force of substorm currents, *Geophys. Res. Lett.*, *25*, 959–962, 1998.

Snyder, A. L., and S.-A. Akasofu, Auroral oval photographs from the DMSP 8531 and 10533 satellites, *J. Geophys. Res.*, *81*, 1799–1804, 1976.

Sofko, G. J., R. Greenwald, and W. Bristow, Direct determination of large-scale magnetospheric field-aligned currents with SuperDARN, *Geophys. Res. Lett.*, *22*, 2041–2044, 1995.

Starkov, G. V., B. V. Rezhenov, V. G. Vorob'ev, Ya. I. Feldstein, and L. I. Gromova, Dayside auroral precipitation structure, *Geomagn. Aeron., Engl. Transl.*, *42*, 176–183, 2002.

Taylor, J. R., S. W. H. Cowley, T. K. Yeoman, M. Lester, R. Greenwald, G. Sofko, J. P. Villain, and R. Lepping, SuperDARN studies of ionospheric convection in response to a northward turning of the IMF on 23 March 1995, *Ann. Geophys.*, *16*, 549–565, 1998.

Torr, M., et al., A far ultraviolet imager for the International Solar-Terrestrial Physics Mission, *Space Sci. Rev.*, *71*, 329–383, 1995.

Troshichev, O. A., Polar magnetic disturbances and field-aligned currents, *Space Sci. Rev.*, *32*, 275–360, 1982.

Troshichev, O. A., E. M. Shishkina, G. Lu, and A. D. Richmond, Relationship of the ionospheric convection reversal to the hard auroral precipitation boundary, *J. Geophys. Res.*, *101*, 15,423–15,432, 1996.

Vasyliunas, V. M., Mathematical models of magnetospheric convection and its coupling to the ionosphere, in *Particles and Fields in the Magnetosphere*, edited by B. M. McCormac, pp. 60–71, D. Reidel, Norwell, Mass., 1970.

Volkov, M. A., and Yu. P. Maltsev, Interchange instability of the inner plasma sheet boundary, *Geomagn. Aeron., Engl. Transl.*, *26*, 671–673, 1986.

Watanabe, M., T. Iijima, and F. J. Rich, Synthesis models of dayside field-aligned currents for strong interplanetary magnetic field By, *J. Geophys. Res.*, *101*, 13,303–13,320, 1996.

Watanabe, M., T. Iijima, M. Nakagawa, T. A. Potemra, L. J. Zanetti, S.-I. Ohtani, and P. T. Newell, Field-aligned current systems in the magnetospheric ground state, *J. Geophys. Res.*, *103*, 6853–6870, 1998.

Yamamoto, T., S. Inoue, N. Nishitani, M. Ozaki, and C.-I. Meng, A theory for generation of the paired Region 1 and Region 2 field-aligned currents, *J. Geophys. Res.*, *101*, 27,199–27,222, 1996.

————————————

D. Chua, Naval Research Laboratory, Washington, D. C., USA.

J. Kangas and A. Kozlovsky, Sodankylä Geophysical Observatory/Oulu Unit, University of Oulu, P.O. Box 3000, FIN-90014 Oulu, Finland. (Alexander.Kozlovsky@oulu.fi)

A. Koustov, Department of Physics and Engineering Physics, University of Saskatchewan, Saskatoon, Saskatchewan, Canada.

W. Lyatsky, Department of Physics, Alabama A&M University, Normal, AL, USA.

G. Parks, Space Science Laboratory, University of California, Berkeley, CA, USA.